Effect of Coagulation Bath Temperature on Formation Mechanism of Poly(vinylidene fluoride) Membrane

Xuyun Wang,[1,2] Lin Zhang,[1] Dahai Sun,[1] Quanfu An,[1] Huanlin Chen[1]

[1]*College of Materials Science and Chemical Engineering, Zhejiang University, Hangzhou, China*
[2]*College of Chemical Engineering, Qingdao University of Science and Technology, Qingdao, China*

Received 10 May 2007; accepted 26 December 2007
DOI 10.1002/app.28169
Published online 28 July 2008 in Wiley InterScience (www.interscience.wiley.com).

ABSTRACT: Effects of coagulation bath temperature on the membrane formation mechanism and the morphologies of the formed membranes were studied. The binodal and spinodal lines in the phase diagrams of water/DMAc/Poly(vinylidene fluoride) (PVDF) were calculated based on the thermodynamics equations of membrane formation, and the gel phase boundaries of the systems at 25°C and 60°C were determined via cloud point measurement. The obtained ternary phase diagrams of water/DMAc/PVDF contain three regions: the one-phase region, the liquid–liquid two-phase region, and the gel region. In the phase diagrams, the liquid–liquid demixing line (binodal) is located inside the gelation line. At low temperature, there exists a wide region between gelation line and binodal line. Gelation could occur in the absence of liquid–liquid demixing, and becomes the dominant membrane formation mechanism. At high temperatures (60°C), however, the gelation line approaches the binodal line, which results in a much smaller gelation zone. The kinetics of the solvent out-flux and water influx were enhanced, liquid–liquid demixing is the dominant mechanism. The membrane formation mechanisms at different temperature were confirmed by the light transmission measurements during membrane forming process and the morphologies of the membranes examined by SEM imaging. © 2008 Wiley Periodicals, Inc. J Appl Polym Sci 110: 1656–1663, 2008

Key words: PVDF; phase diagram; thermodynamics; formation mechanism; morphology

INTRODUCTION

Poly(vinylidene fluoride) (PVDF) is a kind of semicrystalline polymer possessing good chemical resistance and thermal stability. Porous PVDF membrane can be easily produced by immerse precipitation technology for its good dissolving property in a variety of solvents.[1–10] PVDF membranes are widely used in various membrane applications, for example, fuel cells, water purification, wastewater treatment, the petrochemical industry, etc.[11–13] The membrane with the given morphology has been required in different application fields. The morphology and performance of membrane are affected by many membrane formation parameters. Of all these parameters, the concentration of the polymer, additives,[1,3,6,9] solvent,[3] the composition, and the temperature of the coagulation bath[4,7] are the most influential and frequently discussed in literatures. However, most of the studies focus on the influence of the parameters on the morphology of the membranes, the correspondence between theoretical phase diagrams, and experimental phase diagrams is rarely studied. Cheng[7,14] investigated the phase behavior of the membrane forming water/DMF/PVDF and 1-octanol/DMF/PVDF systems, and drew the conclusion that, liquid–liquid demixing took place earlier than crystallization, and cellular asymmetric morphologies were produced at elevated temperatures. At the following conditions, for example, at low temperatures, water was added to the dope to form an ''incipient dope,'' the bath contains a high concentration of DMF, the membrane formed into a uniform particulate structure dominated by the crystallization mechanism. However, the comprehensive membrane formation mechanism for PVDF membrane via immerse precipitation technology need further research.

In the present study, the membrane formation mechanisms at different coagulation bath temperature were studied for water/DMAc/PVDF system. The relationship between theoretical phase diagrams and the morphology of the prepared membranes were attempts to be discussed.

CALCULATION OF TERNARY THERMODYNAMIC PHASE DIAGRAMS

Foundation of the equations

The calculation of thermodynamic phase diagrams of water/DMAc/PVDF system was based on the

Correspondence to: L. Zhang (linzhang@zju.edu.cn).
Contract grant sponsor: the National Basic Research Program of China; contract grant number: 2003CB615706.
Contract grant sponsor: Zhejiang Provincial Natural Science Foundation of China; contract grant number: Y407230.

Flory–Huggins theory[15], the details are given by the following relation:

$$\Delta G_M/RT = n_1 \ln \phi_1 + n_2 \ln \phi_2 + n_3 \ln \phi_3 + g_{12} n_1 \phi_2 + g_{13} n_1 \phi_3 + g_{23} n_2 \phi_2 \quad (1)$$

ΔG_M is the Gibbs free energy of mixing. The subscripts 1,2,3 refer to nonsolvent (1), solvent (2), and polymer (3). n_i and ϕ_i are moles and the volume fraction of component i, respectively. R and T have their usual significance. g_{ij} is the interaction parameter of i and j components.

According to the definition of chemical potentials

$$\frac{\Delta \mu_i}{RT} = \frac{\partial \left(\frac{\Delta G_M}{RT}\right)_{T,P,n_j j \neq i}}{\partial n_i} \quad (2)$$

following equations could be obtained[10–12]:

$$\Delta \mu_1/RT = \ln \phi_1 + 1 - \phi_1 - \frac{v_1}{v_2}\phi_2 - \frac{v_1}{v_3}\phi_3 + (g_{12}\phi_2 + g_{13}\phi_3)(\phi_2 + \phi_3) - g_{23}\frac{v_1}{v_2}\phi_2\phi_3 - u_1 u_2 \phi_2 \left(\frac{dg_{12}}{du_2}\right) - \phi_1 Y_2^3 \left(\frac{dg_{13}}{dY_3}\right) \quad (3)$$

$$\Delta \mu_2/RT = \ln \phi_2 + 1 - \phi_2 - \frac{v_2}{v_1}\phi_1 - \frac{v_2}{v_3}\phi_3 + \left(g_{12}\frac{v_2}{v_1}\phi_1 + g_{23}\phi_3\right)(\phi_1 + \phi_3)\left(\frac{dg_{23}}{dw_3}\right) - g_{13}\frac{v_2}{v_1}\phi_1\phi_3 + u_1 u_2 \frac{v_2}{v_1}\phi_1 \left(\frac{dg_{12}}{du_2}\right) - \phi_2 w_3^2 \quad (4)$$

$$\Delta \mu_3/RT = \ln \phi_3 + 1 - \phi_3 - \frac{v_3}{v_1}\phi_1 - \frac{v_3}{v_2}\phi_2 + \left(g_{13}\frac{v_3}{v_1}\phi_1 + g_{23}\frac{v_3}{v_2}\phi_2\right)(\phi_1 + \phi_2) - g_{12}\frac{v_3}{v_1}\phi_1\phi_2 + \phi_3\left[\frac{v_3}{v_1}Y_1^2\left(\frac{dg_{13}}{dY_3}\right) + \frac{v_3}{v_2}w_2^3\left(\frac{dg_{23}}{dw_3}\right)\right] \quad (5)$$

where v_i is the mole volume of component i, $u_1 = \phi_1/(\phi_1 + \phi_2)$, $u_2 = \phi_2/(\phi_1 + \phi_2)$, $Y_1 = \phi_1/(\phi_1 + \phi_3)$, $Y_3 = \phi_3/(\phi_1 + \phi_3)$, $w_2 = \phi_2/(\phi_2 + \phi_3)$, $w_3 = \phi_3/(\phi_2 + \phi_3)$.

According to the definition of binodal line, the conditions for the equilibrium of polymer dilute phase and polymer concentrated phase are:

$$\Delta \mu_i(\text{concentrated phase}) = \Delta \mu_i(\text{dilute phase}) \Delta C_i = 1, 2, 3 \quad (6)$$

The material balance equations for the dilute and the concentrated phase give another two equations (The subscripts A refers to concentrated phase and B refers to dilute phase respectively):

Concentrated phase:

$$\sum (\phi_{A1} + \phi_{A2} + \phi_{A3}) = 1 \quad (7)$$

Dilute phase:

$$\sum (\phi_{B1} + \phi_{B2} + \phi_{B3}) = 1 \quad (8)$$

The equation for spinodal is:

$$G_{22} \cdot G_{33} = (G_{23})^2 \quad (9)$$

Where

$$G_{ij} = \partial^2 \Delta G_M / \partial \phi_i \partial \phi_j$$

$$G_{22} = \frac{1}{\phi_1} + \frac{v_1}{v_2\phi_2} - 2g_{12} + 2(u_1 - u_2)\left(\frac{dg_{12}}{du_2}\right) + u_1 u_2 \left(\frac{d^2 g_{12}}{du_2^2}\right) - 2Y_3^3 \left(\frac{dg_{13}}{dY_3}\right) + Y_1 Y_3^2 \left(\frac{d^2 g_{13}}{dY_3^2}\right) - \frac{2v_1}{v_2} w_3^2 \left(\frac{dg_{23}}{dw_3}\right) + \frac{v_1}{v_2} w_2 w_3^3 \left(\frac{d^2 g_{23}}{dw_3^2}\right) \quad (10)$$

$$G_{23} = \frac{1}{\phi_1} - (g_{12} + g_{13}) + \frac{v_1}{v_2} g_{23} + u_2(u_1 - 2u_2)\left(\frac{dg_{12}}{du_2}\right) + u_1 u_2^2 \left(\frac{d^2 g_{12}}{du_2^2}\right) + Y_3(Y_1 - 2Y_3)\left(\frac{dg_{13}}{dY_3}\right) + Y_1 Y_3^2 \left(\frac{d^2 g_{13}}{dY_3^2}\right) - \frac{v_1}{v_2} w_2^2 w_3^2 \left(\frac{d^2 g_{23}}{dw_3^2}\right) + \frac{v_1}{v_2} w_2 w_3 (w_3 - w_2)\left(\frac{dg_{23}}{dw_3}\right) \quad (11)$$

$$G_{33} = \frac{1}{\phi_1} + \frac{v_1}{v_3}\frac{1}{\phi_3} - 2g_{13} - 2u_2^3 \left(\frac{dg_{12}}{du_2}\right) + u_1 u_2^3 \left(\frac{d^2 g_{12}}{du_2^2}\right) + 2(Y_1 - Y_3)\left(\frac{dg_{13}}{dY_3}\right) + Y_1 Y_3 \left(\frac{d^2 g_{13}}{dY_3^2}\right) + \frac{2v_1}{v_2} w_2^3 \left(\frac{dg_{23}}{dw_3}\right) + \frac{v_1}{v_2} w_2 w_2^3 \left(\frac{d^2 g_{23}}{dw_3^2}\right) \quad (12)$$

If the interaction parameters are known, and one variable is chosen (ϕ_{A3}), the spinodal line could be obtained combining the material balance equation, $\sum (\phi_1 + \phi_2 + \phi_3) = 1$.

Calculation of interaction parameters

The interaction parameter g_{12} could be calculated from literature data on the excess free enthalpy of mixing, G^E, which are generally obtained from vapor pressure experiments. For a two-component system, G^E is related to the Gibbs free energy of mixing by the equation

$$G^E = \Delta G_m - RT(x_1 \ln x_1 + x_2 \ln x_2) \tag{13}$$

where x_1 and x_2 are the mole fractions of the nonsolvent (1) and the solvent (2). For 1 mol of mixture

$$\Delta G_m/RT = x_1 \ln \phi_1 + x_2 \ln \phi_2 + g_{12} x_1 \phi_2 \tag{14}$$

From eq. (14), g_{12} could be calculated via the relationship with parameter ϕ_2.

The interaction parameter g_{13} could be determined from equilibrium swelling measurements.

$$g_{13} = -\frac{[\ln(1-\phi_3)+\phi_3]}{\phi_3^2} \tag{15}$$

And

$$\phi_3 = \frac{W_{\text{dry}}/\rho_3}{\frac{W_{\text{dry}}}{\rho_3} + \frac{W_{\text{wet}} - W_{\text{dry}}}{\rho_1}} \tag{16}$$

where W_{dry} and W_{wet} are the mass of polymer before and after equilibrium swelling measurement respectively; ρ_1 and ρ_3 are the density of the nonsolvent (1) and the polymer (3).

Method of computation

There are five equations [eq. (6)–(8), three equations included in eq. (6)] and six unknowns (ϕ_{A1}, ϕ_{A2}, ϕ_{A3}, ϕ_{B1}, ϕ_{B2}, ϕ_{B3}) for the computation of binodal line. To determine the tie lines connect the coexisting phases (points on the binodal line), the six unknowns must be determined.

Trivial solutions are usually existed in the computation of binodal line equations. For example, when the volume fractions of different compositions are equal in the dilute phase and in the concentrated phase, the eqs. (6)–(8) are all balanced and infinite solutions existed. To avoid this problem, in general, one variable (for example, ϕ_{A3}) was chosen first as independent variable. Because the volume fraction of polymer in the dilute phase, ϕ_{B3}, was very small, a very small value, for example, 10^{-10}, could be assumed. By changing the value of ϕ_{A3} continually, and substituting the material balance equations into eq. (6) to determine others unknowns, until the solutions of the equations were obtained, and the binodal line was determined.

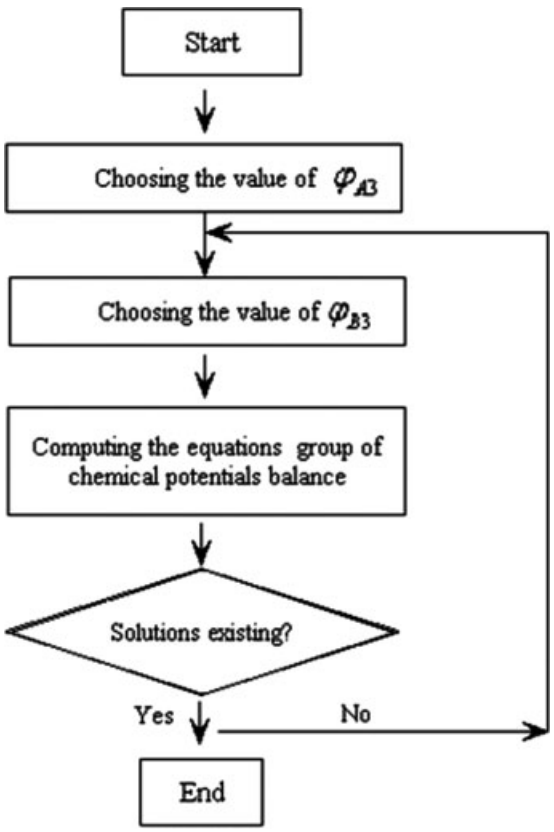

Figure 1 Flow chart of numerical procedure of binodal line.

The flow chart of numerical procedure is shown in Figure 1. A least-squares procedure was used. The objective function is following,

$$F = \sum (f_1^2 + f_2^2 + f_3^2) \tag{17}$$

The numerical computation was carried out via the computing software Matlab 6.5.

The equation group for spinodal line computation was composed by two equations and three unknowns. So, the computation of spinodal line is much easier than that of binodal line. It is also carried out by assuming the volume fraction of polymer. The intersection of binodal line and spinodal line was critical point.

The calculated binodal line and spinodal line of DMAc/PVDF/H_2O ternary system were shown in Figure 2.

EXPERIMENTAL

Materials

PVDF (Shanghai 3F New Materials Co., LTD: intrinsic viscosity = 1.78 dL/g, M_n = 430,000 g/mol) was obtained in powdery form. DMAc (Shanghai SSS Regent Co., LTD, reagent grade, 98 wt %,

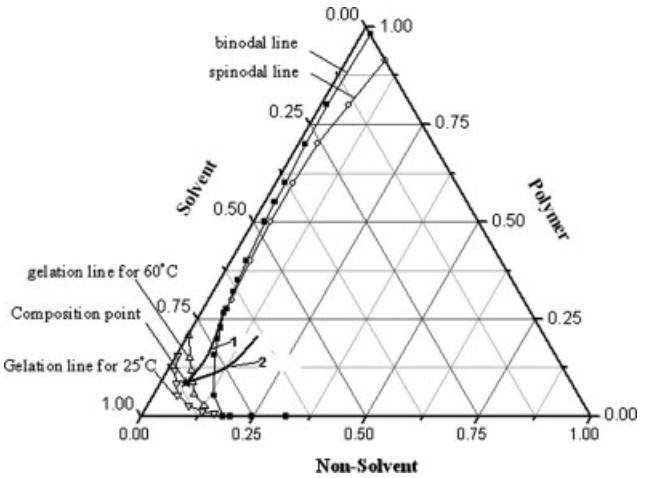

Figure 2 Phase diagram of ternary system of PVDF/DMAc/H_2O.

d = 0.940 g/mL) was used as the solvent. De-ionized water was used as the nonsolvents. All materials were used as received.

Gelation boundary

The gelation boundary at certain temperature of PVDF in water/DMAc solutions was determined by the ''cloud point'' method. A known quantity of nonsolvent was added to a homogeneous PVDF/DMAc solution. The mixture was agitated with a roll mill at elevated temperature until a clear homogeneous solution was obtained. It was then put in a thermostatically controlled oven maintained at certain temperature for a period of 3–5 days. The equilibrium gelation points at certain temperature were identified as the compositions at which homogeneous solutions just began to precipitate into a gel.

Membrane preparation and characterization

Membranes were prepared by immersion precipitation method. A homogeneous dope was cast on a glass plate and subsequently immersed in a coagulation bath. Compositions of the dope are: PVDF: 15 wt %, DMAc: 79 wt %, water: 6 wt %, which represented a homogeneous polymer solution before the state of ''incipient precipitation'' appeared which respects to PVDF crystallization. And 60°C, 25°C, and 15°C de-ionized water were used as coagulation bath separately. The light transmittance through the film as a function of time was measured via a light transmission set-up (Fig. 3).

The formed membranes were soaked in de-ionized water for 1 week and then soaked in ethanol aqueous solution (33%) to remove residual DMAc and then dried in open air.

A field emission scanning electron microscope (SEM) was used to analyze the surface and cross section morphologies of the prepared membrane (XL30ESEM, Belgium). The sample was vacuum-dried and was sputtered with gold films.

The shrinkage ratio of the membrane during dry process could be given as eq. (18):

$$\omega = \frac{S_o - S_d}{S_o} \times 100\% \tag{18}$$

where, ω is the shrinkage ratio of the membrane during dry process, S_o is the area of wet membrane, S_d is the area of dry membrane.

The porosity was measured by immersing the membrane into *n*-Octanol for 2 h, after which the membrane surface was dried by filter paper. The membrane was weighed before and after absorption of the *n*-Octanol. The porosity was calculated using the following equation [eq. (19)]:[16]

$$\varepsilon = \frac{m_n/\rho_n}{m_n/\rho_n + m_p/\rho_p} \times 100\% \tag{19}$$

where, ε is the porosity of the membrane, m_p is the mass of dry membrane, m_n is the mass of absorbed *n*-butanol, ρ_p is the density of PVDF, and ρ_n is the density of *n*-Octanol.

RESULTS AND DISCUSSION

For a given homogeneous casting solution (PVDF: 15 wt %, DMAc: 79 wt %, water: 6 wt %), the prepared membranes show great differences when 60°C, 25°C, and 15°C de-ionized water were used as coagulation bath, respectively. First, the transparence of the membrane prepared using 15°C de-ionized water is larger than that of using 60°C de-ionized water as coagulation bath apparently. Second, the lower temperature of coagulation bath, the larger shrinkage ratio of the membrane is during dry process. The phenomenon is seldom mentioned or explained theoreti-

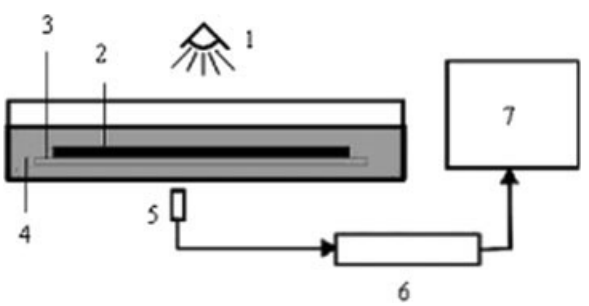

Figure 3 Light set-up: 1. light source; 2. cast polymer film; 3. glass plate; 4.coagulation bath; 5. detector; 6. amplifier; 7. recorder.

TABLE I
Properties of Membranes Prepared at Different Coagulation Bath Temperature

Temperature of coagulation bath (°C)	Shrinkage ratios (%)	Thickness (μm)	Porosity (%)
60	10.0	203	83.1
25	61.4	144	49.5
15	73.5	146	34.0

cally in literatures. The shrinkage ratios of the membranes prepared using 60°C, 25°C, and 15°C de-ionized water as coagulation bath were 10.0%, 61.4%, and 73.5% separately. It was shown in Table I. Moreover, the thickness and porosity of the membrane prepared using 60°C de-ionized water as coagulation bath were much larger than those of the membranes prepared using 25°C and 15°C de-ionized water as coagulation bath, and the differences of the results for 25°C and 15°C were not very large.

The measured light transmission curves using different temperature water as coagulation bath for the same dope compositions was shown in Figure 4. It could be seen that the membrane precipitation process includes two stages, for 25°C and 15°C coagulation bath, in the first stage, the light transmittance decreases slowly; in the second stage, the light transmittance decreases quickly at first, and then the light transmittance decrease speed becomes more and more slowly till the light transmittance is changeless at last. The lower of the coagulation bath temperature, the longer of the first stage last. At 25°C and 15°C, the first stage lasted about 90 and 180 s, respectively. For the 60°C coagulation bath, in the first stage, the light transmittance decreases very quickly in a few seconds after the membrane was immersed into the coagulation bath, and about 20 s later, the second stage starts. Moreover, during the experiment process, it could be observed that the turning point of the two stages corresponding to the solidification moment of the film, and the membrane lifts off the glass plate.

According to the above-mentioned experiment results, it could be drawn the conclusion that there are two types different mechanism exist in the PVDF/DMAc/H_2O system during the membrane formation by immersion precipitation phase inversion techniques. One is liquid–liquid demixing, the other is gelling demixing, and at low temperature, the later is prior the former.

Phase diagrams of PVDF/DMAc/H_2O system are given in Figure 2. The data points on the gel line represent the measured compositions at which gelation were observed at different temperature. When the composition point of the system locates the top right side of the gel line, crystallization-induced gelation would occur first for an initially uniform solution. As the temperature was raised, gels formed at lower temperatures may fuse into homogeneous solutions. Hence, the gelation boundaries shift upward and rightward with increasing temperature (ex. 60°C), and shift nearer to the binodal line.

At low temperature (ex.15°C and 25°C), the composition point (PVDF: 15 wt %, DMAc: 79 wt %, water: 6 wt %) of the system locates in the gelation region (changed into v% already) in Figure 2, so physical gelation occurred first in the membrane formation processes, the schematic composition path of the cast film after immersion as line 1 shown in Figure 2, which is above-mentioned gelling demixing stage. During this stage, the liquid–liquid de-mixing induced by kinetics of the solvent out-flux and water influx was very slow, so the light transmission experiment results (Fig. 4) shown that, the delayed liquid–liquid de-mixing occurred at low temperature. Here, the gelation is, in fact, not a phase separation process, and it takes place in a homogeneous system in the experiment, forms a solid phase consisting of the polymer PVDF and the solvent DMAc. Actually, the formed solid phase is a swelling condition of PVDF in solvent. So, much solvent was solidified in the three dimensional polymer chains fibriform network of gelation and couldn't be exchanged with the nonsolvent, and during drying process, the solvent solidified in the membrane will volatilize to the air, the polymer chains of fibriform network shrinks for the action of flexibility shrinkage energy, and that results the serious shrinkage of the prepared membranes. The same reason could also explain that, why the thickness and the porosity of the membranes prepared using 15°C de-ionized water as coagulation bath are much less than those of using 60°C water.

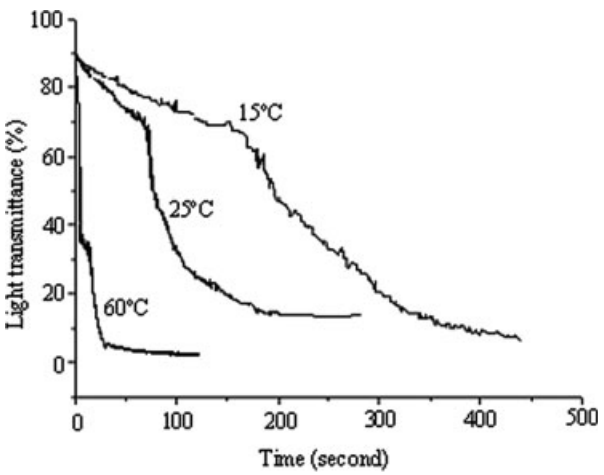

Figure 4 Light transmission measurements of the PVDF/DMAc/H_2O system casting solution immersing in (a) 15°C, (b) 25°C, and (c) 60°C de-ionized water.

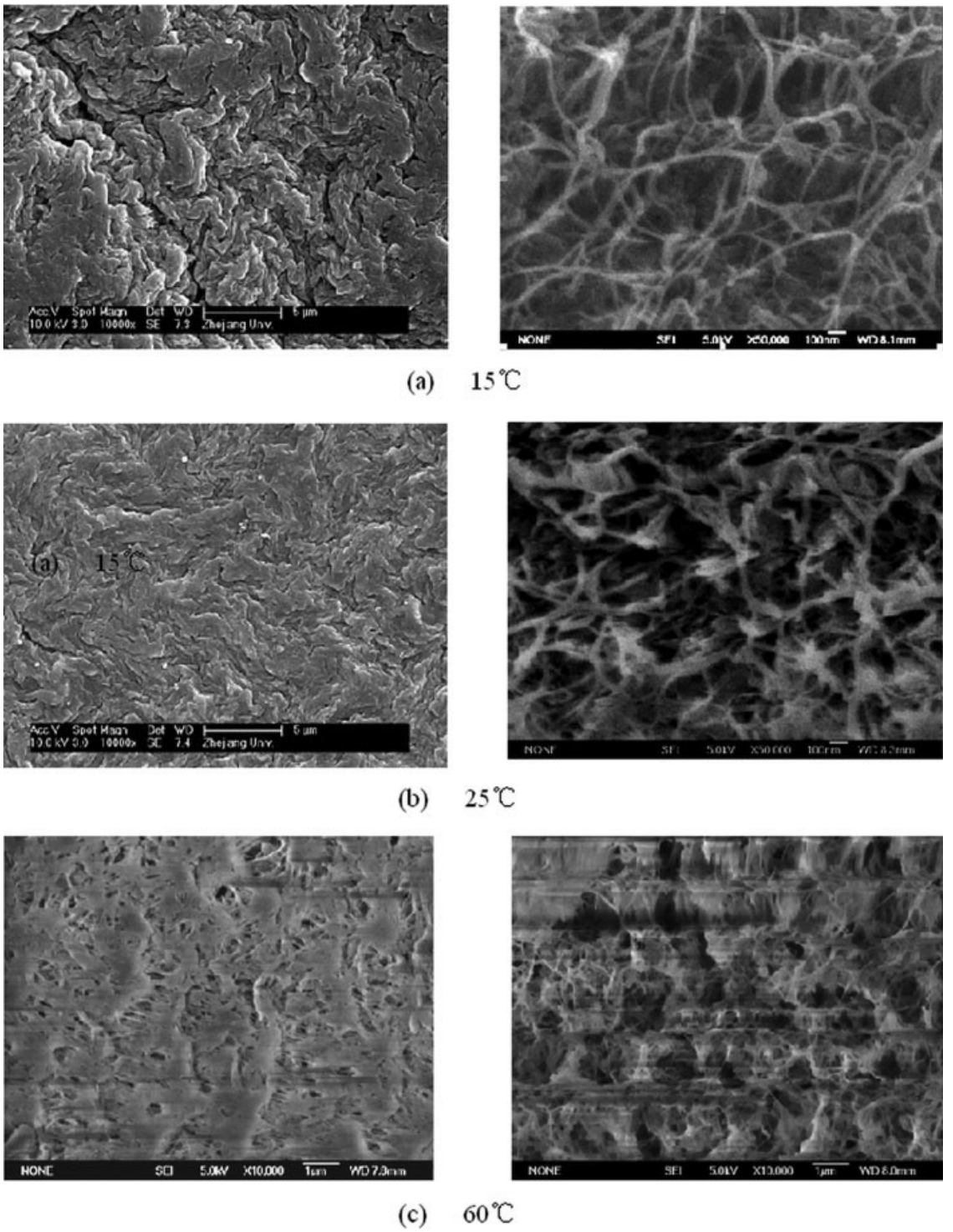

Figure 5 SEM micrographs of the PVDF membranes prepared by immersion in (a) 15°C, (b) 25°C, and (c) 60°C de-ionized water, left: top surface, right: cross section.

At a high temperature (ex. 60°C), the gelation boundaries shift nearer to the binodal line (Fig. 2), and the kinetics of the solvent out-flux and water influx were enhanced, which suppressed gelation but favored liquid–liquid de-mixing. Especially, the addition of nonsolvent (water) to the polymer solution results the composition of the casting solution lies close to the binodal and spinodal line. So, during the membrane formation process, the composition path would cross the gelation region and binodal line instantaneously (the gelation region and binodal line are nearly overlapped at low polymer concentration), as line 2 shown in Figure 2, and liquid–liquid demixing would start in this case. The light trans-

mission experiment results (Fig. 4) shown that, liquid–liquid demixing occurs in a very short time. Moreover, much little eddy could be observed above the film after the polymer solution was cast upon a glass plate and immersed in 60°C water. With the out-fluxing of the solvent from the membrane, the concentration of the rich polymer phase becomes so high that solidification occurs, then, the membrane lifts off the glass plate and is no longer transparent in a short time. Because the formed membranes were soaked in de-ionized water for 1 week and then soaked in ethanol aqueous solution (33%) to remove residual DMAc before dried, so the shrinkage ratios of the prepared membrane is very little (see Table I), and the thickness and porosity of the membrane is comparatively large.

The above-mentioned different membrane formation mechanisms at different coagulation bath temperature could be validated according to the morphology of the prepared membrane. In general, a dense top-layer and cellular substrate morphology was obtained if the delayed liquid–liquid demixing take place for PVDF membrane. However, the substrate morphology of the prepared membranes is three dimensional fibriform network (see Fig. 5a,b) at low coagulation bath temperatures (15°C and 25°C). Because PVDF is a semicrystalline polymer, at low temperature, the gelation initiated by the formation of microcrystallites occurs before liquid–liquid demixing. These microcrystallites could connect various polymeric chains together, and form a three dimensional fibriform network. Moreover, serious shrinkage of the prepared membrane during drying process results in dense and wizened surface. In general, at high coagulation bath temperature (ex. 60°C), the composition path of the cast film cross the gelation region, binodal line and spinodal instantaneously, start liquid–liquid demixing, and form the high connected rich polymer phase and poor polymer phase. After the solidification of the polymer phase, high connected fibriform or leaf-form network substrate morphology membrane could be obtained (see Fig. 5c,b).

CONCLUSIONS

Different coagulation bath temperature could attribute to different membrane formation mechanisms during PVDF membrane formation process by immersion precipitation method. There are two types of membrane formation mechanism in the process, one is liquid–liquid demixing, and the other is gelation.

The phase diagram of water/DMAc/PVDF ternary system contains three regions: the one-phase region, the liquid–liquid two-phase region and the gel region. At low temperature (15°C and 25°C), the composition point of the system locates in the gelation region, and physical gelation occurs first in the membrane formation processes. The liquid–liquid de-mixing induces by kinetics of the solvent out-flux and water influx is very slow, and gelation is the dominate membrane formation mechanism.

At high temperature (60°C), the gelation boundaries shift nearer to the binodal line, and the kinetics of the solvent out-flux and water influx are enhanced, which suppresses gelation but favors liquid–liquid de-mixing, and then liquid–liquid demixing is the dominate mechanism.

The different membrane formation mechanisms are validated by the light transmission measurements during membrane formation process and the morphology of the prepared membrane.

NOMENCLATURE

ΔG	Gibbs free energy kJ•kmol^{-1}
ϕ	volume fraction
T	Temperature (K)
$\Delta\mu$	Chemical potential
n	moles fraction
R	Universal gas constant (8.314 kJ•kmol^{-1}•K^{-1})
g_{ij}	Interaction parameter of i-j components
ν	Moles volume
ω	Shrinkage ratio
ε	Porosity
ρ	Density kg•m^{-3}
S	Area of membrane, m^2
m	Mass, kg,

Subscripts

M	Mixture
A	Concentrated phase
o	wet membrane
p	polymer
i	Component
B	Dilute phase
d	dry membrane
n	n-Octanol

References

1. Lin, D.; Chang, C. L.; Huang, F. M.; Cheng, L. P. Polymer 2003, 44, 413.
2. Bottino, A.; Capannelli, G.; Comite, A. Desalination 2005, 183, 891.
3. Yeow, M. L.; Liu, Y. T.; Li, K. J Appl Polym Sci 2004, 92, 1782.
4. Deshmukh, S. P.; Li, K. J Membr Sci 1998, 150, 75.
5. Khayet, M.; Matsuura, T. Ind Eng Chem Res 2001, 40, 5710.
6. Khayet, M.; Feng, C. Y.; Khulbe, K. C.; Matsuura, T. Desalination 2002, 148, 321.

7. Cheng, L. P. Macromolecules 1999, 32, 6668.
8. Wang, D.; Li, K.; Teo, W. K. J Membr Sci 1999, 163, 211.
9. Wang, D.; Li, K.; Teo, W. K. J Membr Sci 2000, 178, 13.
10. Lin, D. J.; Beltsios, K.; Young, T. H.; Jeng, Y. S.; Cheng, L. P. J Membr Sci 2006, 274, 64.
11. Qin, J. J.; Wai, M. N.; Tao, G.; Kekre, K. A.; Seah, H. Sep Purif Technol 2007, 53, 296.
12. Gopal, R.; Kaur, S.; Ma, Z.; Chan, C.; Ramakrishna, S.; Matsuura, T. J Membr Sci 2006, 281, 581.
13. Gao, K.; Hu, X.; Dai, C.; Yi, T. Mater Sci Eng B 2006, 131, 100.
14. Cheng, L. P.; Lin, D. J.; Shih, C. H.; Dwan, A. H.; Gryte, C. C. J Polym Sci B: Polym Phys 2079 1999, 37.
15. Altena, F. W.; Smolders, C. A. Macromolecules 1982, 15, 1491.
16. Wang, Y. J.; Kim, D. Electrochim Acta 2007, 52, 3181.